

Open Quantum Dynamics Theory for Coulomb Potentials: Hierarchical Equations of Motion for Atomic Orbitals (AO-HEOM)

Yankai Zhang[Ⓛ] and Yoshitaka Tanimura^{Ⓛ^a}

Department of Chemistry, Graduate School of Science, Kyoto University, Kyoto 606-8502, Japan

(Dated: Last updated: 18 March 2026)

We investigate the quantum dynamics of Coulomb potential systems in thermal baths. We study these systems within the framework of open quantum dynamics theory, focusing on preserving the rotational symmetry of the entire system, including the baths. Thus, we employ a three-dimensional rotationally invariant system-bath (3D-RISB) model to derive numerically “exact” hierarchical equations of motion for atomic orbitals (AO-HEOM) that enable a non-perturbative and non-Markovian treatment of system-bath interactions at finite temperatures. To assess the formalism, we calculated the linear absorption spectrum of an atomic system under isotropic thermal environment, with systematic variation of system-bath coupling strength and temperature.

I. INTRODUCTION

Coulomb potentials encompass a wide variety of physical systems characterized by interactions among charged particles.^{1–3} The potential typically follows an inverse radial dependence, $\propto 1/r$, where r is the distance from the charge center. To account for short-range interactions, a correction term of the form $\propto e^{-r/\rho}/r^n$ is often included, with ρ denoting the screening length and n an integer exponent. Hydrogen atoms are a well-known example, but the same potential has also been applied to problems in condensed phases, such as the color center problem in ionic crystals, where an anion vacancy traps an electron, forming a point defect,^{4–6} and to interactions between ions in ionic solvents.^{7,8}

Recent advances in CPU power and algorithmic development have enabled the efficient dynamic simulation of isolated Coulomb systems, despite the persistence of certain mathematical challenges.⁹ In contrast, simulating quantum dynamics under the influence of thermal environments (baths) remains a significant challenge. This difficulty has been circumvented in the case of vacuum radiation fields as a bath, where thermal excitations are absent. Indeed, such scenarios represent one of the earliest applications of open quantum dynamics theory. In such cases, the system-bath (S-B) coupling is weak, and the quantum effects of thermal fluctuations are negligible due to the much larger excitation energy compared to the thermal energy. Under these conditions, several assumptions become valid, including the rotating wave approximation (RWA), the factorized assumption (FA), and the Markovian approximation. These allow the qualitative influence of the bath to be incorporated into the dynamics of the energy eigenstates of the system, with relaxation processes characterized by transition rates, typically expressed in terms of Einstein coefficients.^{10,11} Ide-

ally, natural radiation damping in atomic systems is governed by the full Hamiltonian describing Coulomb interactions with a surrounding bath. Yet, under perturbative and Markovian assumptions, a simplified S-B model can accurately capture the essential features of the relaxation process.

In condensed phases, where thermal excitations play a crucial role, a non-Markovian treatment of fluctuation-dissipation theorem, is significant.^{12–15} Over the past three decades, it has been recognized that applying the Markov assumption to spin-Boson systems with the Ohmic spectral distribution function (SDF) under thermal conditions leads to unphysical anomalies—notably, equal populations of ground and excited states regardless of temperature.^{16–20} These results indicate inherent limitations in the thermal treatment, provided by the Lindblad-master,^{21–24} the Markovian-Redfield,²⁵ and the quantum Fokker–Planck equations.^{26,27} Such inconsistencies can be resolved using the numerically “exact” hierarchical equations of motion (HEOM)^{12–15} and the quasi-adiabatic path-integral (QUAPI) approach,^{28–30} both of which are non-perturbative and non-Markovian frameworks that rigorously and quantitatively account for the influence of thermal environment.

However, a more fundamental question remains: What is the appropriate characterization of heat baths that interact with Coulombic systems exhibiting rotational symmetry? To gain deeper insight into this issue, here we introduce the three-dimensional rotationally invariant system-bath (3D-RISB) model. This framework, developed to investigate quantum rotors^{31–35} and Aharonov–Bohm (AB) rings,^{36,37} extends a two-dimensional (2D) predecessor originally proposed for current-biased tunnel junctions.³⁸ The present study extends the RISB model to examine the dynamics of systems with atomic orbits that exhibit rotational symmetry.

Notably, even when employing the 3D-RISB model, the quantum Fokker–Planck equation^{26,27}—applicable only at elevated temperatures—proves inadequate in re-

^{a)} Author to whom correspondence should be addressed: tanimura.yoshitaka.5w@kyoto-u.jp

producing key quantum effects, as evidenced by the AB ring analysis.^{36,37} While the 3D-RISB model entails significant computational cost, the HEOM formalism, which robustly handles low-temperature dynamics, remains indispensable for addressing the class of quantum transport problems explored in this study. The capability of HEOM to treat non-perturbative S-B coupling also offers the advantage of enabling research into a wide range of problems, including cavity quantum electrodynamics (cavity QED), where atoms or nanomaterials are coupled to intense electromagnetic fields within small cavities.^{39–46}

Recent developments in the HEOM formalisms include QHFPE (quantum hierarchical Fokker–Planck equations),^{47,48} MB-HEOM (HEOM for multiple baths),²⁰ and U(1)-HEOM (HEOM with U(1)-Gauge fields),³⁷ with corresponding numerical implementations made available. In this study, we introduce a new variant—HEOM for atomic orbitals (AO-HEOM)—which is structurally and conceptually distinct from existing HEOM, characterized by its incorporation of three spatially distributed, independent thermal baths. The AO-HEOM code developed herein, which fully utilizes the graphics processing unit (GPU),^{49,50} will be made publicly available in a separate work. To validate our theoretical framework, we compute the linear absorption spectrum of the Coulomb system across a range of bath temperatures and coupling strengths.

This paper is organized as follows. In Sec. II, we highlight the intrinsic difficulty of modeling a Coulomb system in a thermal environment within standard open-quantum dynamics frameworks. This motivates the introduction of the 3D-RISB model and the subsequent development of the AO-HEOM formalism. A numerical demonstration is given in Sec. III. Section IV is devoted to concluding remarks.

II. OPEN QUANTUM DYNAMICS THEORY FOR COULOMB POTENTIAL SYSTEM

A. Anomaly of Markovian equations and the emergent role of bathentanglement

It is crucial to emphasize that although the Ohmic SDF has been assumed for the study of Markovian dynamics in the spin-boson system, this model exhibits anomalous dynamical behavior (an infrared anomaly) at finite temperatures.^{16–20} This arises because quantum thermal noise is inherently non-Markovian in nature because its correlation time and amplitude must satisfy the uncertainty principle.^{19,20} Even if S-B interactions are weak, there are multiple interactions between the system and the bath during the noise correlation time in non-Markovian cases, requiring a non-perturbative treatment. Consequently, the coherence between the system and bath becomes entangled—a phenomenon we refer to as “bathentanglement” to distin-

guish it from other forms of entanglement.¹⁵ This leads to system dynamics that deviate markedly from those predicted under the factorized assumption. A complementary definition of bathentanglement is $\delta\rho_{B_e}(t) \equiv \rho_{\text{tot}}(t) - \rho_A(t)\rho_B(t)$, where $\rho_{\text{tot}}(t)$ is the full S-B density operator, $\rho_A(t) = \text{tr}_B\{\rho_{\text{tot}}(t)\}$ is the reduced system part, and $\rho_B(t)$ denotes the bath state in the absence of a S-B interaction. Note that for quantum systems formulated in phase space—such as the Brownian harmonic system—bathentanglement vanishes in the high-temperature limit due to the classical nature of the environment, as indicated by the analytical solution of the equilibrium distribution for the quantum harmonic oscillator.⁴⁷ In 2D spectroscopy, the change in peak profiles due to vibrational dephasing is a representative effect of bathentanglement.⁵¹

Neglecting this effect leads to the positivity problem, wherein the diagonal elements of the density operator become negative. Consequently, both the Lindblad-master equation (LME)^{21–24} and the Markovian-Redfield equation (MRE)²⁵ yield unphysical predictions, especially in the low-temperature regime where their foundational assumptions—such as the RWA and the FA condition—fail.^{19,20} Although the time-convolutionless (TCL) Redfield (or Shibata) equation^{52,53} captures non-Markovian noise, its factorized treatment inevitably disrupts bathentanglement, resulting in the violation of the positivity condition.⁴⁷

The quantum Fokker–Planck equation (QFPE),^{26,27} when formulated the system in phase space under the Markov approximation, behaves reliably at high temperatures where classical dynamics dominate. However, at low temperatures, it fails to preserve positivity due to its omission of bathentanglement—S-B correlations stemming from non-Markovian behavior encoded in Matsubara frequency components.¹⁹ Thus, while the Liouvillian remains unchanged between classical and quantum harmonic systems, the bathentanglement introduces \hbar into its thermal equilibrium distribution, reflecting quantum coherence effects.⁴⁷ These analyses were conducted for the spin-boson model¹⁶ or the Caldeira–Leggett (CL) model.²⁶ However, as we will discuss below, extending these models to include multiple baths suffers from the same limitations.

B. Rotation symmetry breaking in the CL model

When the bath is modeled as a 3D electro-magnetic field, the total Hamiltonian naturally preserves translational and rotational invariance. In contrast, the standard harmonic oscillator bath used to incorporate thermal effects lacks this symmetry by construction: While the CL model—classically equivalent to Langevin dynamics—is commonly used to describe rotational relaxation, it fails to reproduce discrete rotational bands in the quantum regime, even under weak S-B coupling in both 2D and 3D cases.^{31–37} This failure stems from the

periodicity of the rotational coordinates: a change from θ to $\theta + 2\pi$ of the system coordinate does not correspond to a change from x_j to $x_j + \delta x_j$ in the bath coordinates, leading to the destruction of bathentanglement. Thus, conventional approaches—including the QFPE^{26,27} and RME^{21,22} or even analytically exact solution^{31,32} derived from the CL model—fail to reproduce discretized transition peaks characteristic of a rotationally invariant system.^{31–37} These computational results are nearly indistinguishable from their classical counterparts, indicating that the loss of rotational bathentanglement renders the dynamics effectively semi-classical.

This problem worsens further for atomic systems with radial degrees of freedom, where electron motion in the Coulomb field reverts to a pre-Bohr classical description: angular momentum loss due to friction pulls the electron toward the potential center. Such behavior reflects the breakdown of bathentanglement. Approaches based on the semi-classical bath—e.g., QFPE^{26,27} and its overdamped limit, the Zusman equation^{54,55}—likewise fail to yield discrete spectra.

C. The 3D-RISB model

Systems exhibiting rotational symmetry are expected to possess periodical quantum coherence. Consequently, the total system—including the bath—must preserve rotational symmetry. To accommodate this requirement, 2D-RISB and 3D-RISB models have been developed.^{33,34} In the classical limit, these models converge to the classical Brownian rotor system, thereby providing a unified framework that seamlessly bridges quantum and classical regimes.

The 3D-RISB model is expressed in a Cartesian coordinate system as

$$\hat{H}_{tot} = \hat{H}_S + \sum_{\alpha=x,y,z} \hat{H}_{I+B}^{\alpha}, \quad (1)$$

where the primary system involved the Coulomb potential, which is defined by

$$\hat{H}_S = \sum_{\alpha=x,y,z} \frac{\hat{p}_{\alpha}^2}{2m_e} - \frac{Z_p e^2}{4\pi\epsilon_0 r}, \quad (2)$$

where \hat{p}_{α} is the momentum operator in the $\alpha = x, y,$ and z direction and m_e is the mass of the system. The Coulomb potential is expressed in terms of the radius from the center of charge, denoted by $r \equiv \sqrt{x^2 + y^2 + z^2}$ and Z_p is the number of positive charge, e is the elementary charge, and ϵ_0 is vacuum permittivity. In this work, we consider the case $Z_p = 1$. The primary system is independently coupled to three heat baths in the $x, y,$ and z directions (3D baths) expressed as^{33–36}

$$\hat{H}_{I+B}^{\alpha} = \sum_j \left\{ \frac{(\hat{p}_j^{\alpha})^2}{2m_j^{\alpha}} + \frac{1}{2} m_j^{\alpha} (\omega_j^{\alpha})^2 \left(\hat{q}_j^{\alpha} - \frac{c_j^{\alpha} \hat{V}_{\alpha}}{m_j^{\alpha} (\omega_j^{\alpha})^2} \right)^2 \right\}, \quad (3)$$

where m_j^{α} , \hat{p}_j^{α} , \hat{q}_j^{α} and ω_j^{α} represent the mass, momentum, coordinate, and frequency, respectively, of the j th bath oscillator mode in the α direction.

These baths can be interpreted as effective environments originating from local interactions with surrounding molecules, electromagnetic fields, or phonon environment. The system part of the S-B interactions is, for example, defined as $(\hat{V}_x, \hat{V}_y, \hat{V}_z) \equiv (\hat{x}, \hat{y}, \hat{z})$, and c_k^{α} is the S-B coupling constant. We include the counter terms that are introduced to maintain the translational symmetry of the system Hamiltonian.⁵⁶ The harmonic bath in the α direction is characterized by the SDF, defined as $J^{\alpha}(\omega) = \sum_k [\hbar(c_k^{\alpha})^2 / 2m_k^{\alpha} \omega_k^{\alpha}] \delta(\omega - \omega_k^{\alpha})$, and the inverse temperature, $\beta \equiv 1/k_B T$, where k_B is the Boltzmann constant.

To adapt the HEOM formalism, we use the Drude SDF expressed as^{14,15}

$$J^{\alpha}(\omega) = \frac{\hbar\eta_{\alpha}}{\pi} \frac{\gamma_{\alpha}^2 \omega}{\gamma_{\alpha}^2 + \omega^2}, \quad (4)$$

where $\alpha = x, y,$ and z . It should be noted that $J^{\alpha}(\omega)$ does not have to be identical for different α directions. In particular, they will differ when the surrounding environment is anisotropic. Such a situation may also be achieved by applying a Stark electric field oriented along a specific axis.³⁴ Alternatively, directional coupling in the xy plane, for example, can be induced by correlating bath modes along the $\alpha = x$ and y directions, thereby introducing anisotropy.⁵⁷

D. AO-HEOM

Preserving bathentanglement—a quintessentially quantum phenomenon—requires low-temperature environments that are inherently non-Markovian. As illustrated in Sec. II A, invoking the Markovian assumption in such contexts can significantly compromise the quantum integrity of the system. Indeed, as evidenced by the analysis of the AB ring system,^{36,37} even with the QHFPE with RISB model fails to reproduce key quantum features such as the AB persistent current in high temperature regime.³⁶ Therefore, the exploration of low-temperature dynamics using HEOM formalism remains indispensable for addressing the various problems examined in this study. Note that, although the HEOM rigorously captures quantum effects, systems formulated in phase space—such as the present model—exhibit only classical features at high temperatures, reflecting the classical nature of the bath in this regime.³⁶

The HEOM provides a non-Markovian and non-perturbative approach to accurately simulate dynamics.^{12–15} The hierarchical structure was introduced to describe the bathentanglement that arises from multiple interactions with the heat bath.^{14,15} In this paper, we adopt the $[K_{\alpha} - 1/K_{\alpha}]$ Padé approximation, where K_{α} is an integer in the α direction, to express the fluctuation and dissipation operators.⁵⁸ The HEOM

in terms of Padé approximated frequency ν_k^α , where $k = \{0, 1, \dots, K_\alpha\}$ with $\nu_0^\alpha = \gamma_\alpha$, are then expressed as^{33,34}

$$\begin{aligned} \frac{d}{dt} \hat{\rho}_{\{\mathbf{n}_\alpha\}} = & - \left[\frac{i}{\hbar} \hat{H}_S^\times + \sum_{\alpha=x,y,z} \sum_{k=0}^{K_\alpha} (n_k^\alpha \nu_k^\alpha) \right] \hat{\rho}_{\{\mathbf{n}_\alpha\}} \\ & - \frac{i}{\hbar} \sum_{\alpha=x,y,z} \sum_{k=0}^{K_\alpha} n_k^\alpha \hat{\Theta}_k^\alpha \hat{\rho}_{\{\mathbf{n}_\alpha - \mathbf{e}_\alpha^k\}} \\ & - \frac{i}{\hbar} \sum_{\alpha=x,y,z} \sum_{k=0}^{K_\alpha} \hat{V}_\alpha^\times \hat{\rho}_{\{\mathbf{n}_\alpha + \mathbf{e}_\alpha^k\}}, \end{aligned} \quad (5)$$

where $\{\mathbf{n}_\alpha\} \equiv (\mathbf{n}_x, \mathbf{n}_y, \mathbf{n}_z)$ is a set of integers $\mathbf{n}_\alpha = (n_0^\alpha, n_1^\alpha, n_2^\alpha, \dots, n_{K_\alpha}^\alpha)$ to describe the hierarchy elements and $\{\mathbf{n}_\alpha \pm \mathbf{e}_\alpha^k\}$ with the index k , where \mathbf{e}_α^k is the k th unit vector in the α direction. We introduced the hyper operators $\hat{A}^\times \hat{B} \equiv \hat{A} \hat{B} - \hat{B} \hat{A}$ and $\hat{A}^\circ \hat{B} \equiv \hat{A} \hat{B} + \hat{B} \hat{A}$, for any operator \hat{A} and \hat{B} , and $\hat{\Theta}_k^\alpha$ is defined as

$$\hat{\Theta}_0^\alpha = \frac{\eta_\alpha \gamma_\alpha}{\beta} \left(1 + \sum_{k=1}^{K_\alpha} \frac{2\eta_k \gamma_\alpha^2}{\gamma_\alpha^2 - \nu_k^{\alpha 2}} \right) \hat{V}_\alpha^\times - \frac{\eta_\alpha \gamma_\alpha}{2} (\hat{H}_S^\times \hat{V}_\alpha)^\circ, \quad (6)$$

and

$$\hat{\Theta}_{k \neq 0}^\alpha = -\frac{\eta_\alpha \gamma_\alpha^2}{\beta} \frac{2\eta_k \nu_k^\alpha}{\gamma_\alpha^2 - \nu_k^{\alpha 2}} \hat{V}_\alpha^\times, \quad (7)$$

where η_α and γ_α are anisotropic coupling strength and inverse noise correlation time. In Eq. (5), $\hat{\rho}_{\{\mathbf{n}_\alpha\}}$ are auxiliary operators with a hierarchical structure. The zeroth member of the hiracial elements $\hat{\rho}_{\{\mathbf{n}_\alpha=0\}}$ represents original reduced density operator. As $(\mathbf{n}_x, \mathbf{n}_y, \mathbf{n}_z)$ can take all combinations of non-negative integers, the HEOM should be closed by ‘‘terminator’’¹³

$$\sum_{\alpha=x,y,z} \sum_{k=0}^{K_\alpha} (n_k^\alpha \nu_k^\alpha) \hat{\rho}_{\{\mathbf{n}_\alpha\}} = -\frac{i}{\hbar} \sum_{\alpha=x,y,z} \sum_{k=0}^{K_\alpha} n_k^\alpha \hat{\Theta}_k^\alpha \hat{\rho}_{\{\mathbf{n}_\alpha - \mathbf{e}_\alpha^k\}} \quad (8)$$

for $\sum_{\alpha=x,y,z} \sum_{k=0}^K (n_k^\alpha \nu_k^\alpha) \gg \Delta\omega_{\max}$, where $\Delta\omega_{\max}$ is the largest transition frequency.

We now introduce spherical coordinates (r, θ, ϕ) . The system part of the S-B interactions in the linear coupling case is expressed as $(\hat{V}_x, \hat{V}_y, \hat{V}_z) \equiv (r \sin(\theta) \cos(\phi), r \sin(\theta) \sin(\phi), r \cos(\phi))$. This formulation may also effectively capture atomic interactions with electromagnetic fields in blackbody environments. Nanomaterials coupled to strong fields in microcavities have recently emerged as key platforms in cavity QED.^{39–46} The AO-HEOM formalism is capable of treating such systems in a non-perturbative manner, even accounting for gauge fields.^{36,37}

The eigenfunctions of the Coulomb potential system are expressed as the product of radial wavefunctions, $R_{nl}(r)$, and spherical harmonics, $Y_{lm}(\theta, \phi)$, as

$$\psi_{n,l,m}(r, \theta, \phi) = R_{nl}(r) Y_{lm}(\theta, \phi), \quad (9)$$

n \ n'	2	3	4	5	Series
1	0.375	0.44444	0.46875	0.48	Lyman
2		0.06944	0.09375	0.105	Balmer
3			0.02430	0.03555	Paschen
4				0.01125	Brackett

TABLE I. Frequencies $\omega_{nn'}$ and absorption transition series from the initial state n to the final states n' (within $n' = 5$) in a Coulomb potential system, evaluated using Eq. (12) with $R = 1/2$ [a.u.]

where n , l , and m are the principal, angular momentum, and magnetic quantum numbers, respectively. We describe the eigenvector for this set of numbers as $|\{\Gamma\}\rangle = | \{n, l, m\} \rangle$. Then the HEOM elements are expressed as $\hat{\rho}_{\{\mathbf{n}_\alpha\}}(\Gamma, \Gamma'; t)$. Any operators such as \hat{H}_S and \hat{V}_α are expressed in terms of matrix elements as $H_S(\Gamma, \Gamma') = \langle \Gamma | \hat{H}_S | \Gamma' \rangle$ and $V_\alpha(\Gamma, \Gamma') = \langle \Gamma | \hat{V}_\alpha | \Gamma' \rangle$.

E. Linear absorption spectrum

We demonstrate our formalism by depicting linear absorption spectrum, defined as³⁴

$$I_{\alpha'\alpha}(\omega) = \text{Im} \left(\frac{i}{\hbar} \right) \int_0^\infty dt e^{i\omega t} \text{Tr} \left\{ \hat{\mu}_{\alpha'} \hat{\mathcal{G}}(t) \hat{\mu}_\alpha^\times \hat{\rho}_{\text{eq}} \right\}, \quad (10)$$

where $\alpha = x, y$, and z , and $\hat{\mu}_x = \mu_0 \sin(\theta) \cos(\phi)$, $\hat{\mu}_y = \mu_0 \sin(\theta) \sin(\phi)$, and $\hat{\mu}_z = \mu_0 \cos(\phi)$, are the dipole operators and $\hat{\mathcal{G}}(t)$ is Green’s function in the absence of a laser interaction, evaluated from Eqs. (5), and $\hat{\rho}_{\text{eq}}$ is the equilibrium density operator. Hereafter, we set $\mu_0 = 1.0$.

In the reduced equation of motion approach, the density matrix is replaced by a reduced one. In the HEOM case, $\hat{\rho}_{\text{tot}}^{eq}$ is replaced by the hierarchy member $\hat{\rho}_{\{\mathbf{n}_\alpha\}}^{eq}(t)$. The Liouvillian in $\hat{\mathcal{G}}(t)$ is replaced using Eqs. (5)-(8).

We evaluate Eqs. (10) in the following five steps.^{14,15} (i) We first run the computational program to evaluate Eqs. (5)-(8) for sufficiently long times from the temporal initial conditions to obtain a true thermal equilibrium state, the full hierarchy members $\hat{\rho}_{\{\mathbf{n}_\alpha\}}^{eq}$ are then used to set the correlated initial thermal equilibrium state. (ii) The system is excited by the first interaction $\hat{\mu}^\times$ at $t = 0$. (iii) The evolution of the perturbed elements is then computed by running the program for the HEOM up to time t . (iv) Finally, the response functions defined in Eq. (10) is calculated as the expectation value of $\hat{\mu}$. A fast Fourier transform yields the spectrum.

For reference, we also depict the absorption spectrum without the bath. From Fermi's golden rule, this is given by

$$I_{\alpha'\alpha}(\omega) = \sum_{n,n'} \mu_{\alpha'}^{n'n} \mu_{\alpha}^{nn'} \frac{e^{-\beta E_{n'}} - e^{-\beta E_n}}{Z} \times \delta(\hbar\omega + E_{n'} - E_n) \quad (11)$$

where $Z = \sum_n e^{-\beta E_n}$ is the partition function and $\mu_{\alpha}^{n'n} = \langle n' | \hat{\mu}_{\alpha} | n \rangle$.

Throughout this paper, we use the basis given in Eq. (9) for the Coulomb potential system Eq. (2). Then the electronic transitions obey selection rules, allowing only transitions with angular momentum and magnetic quantum numbers $\Delta l = \pm 1$, $\Delta m = 0, \pm 1$. However, the peak positions in the absorption spectrum are determined solely by the difference in principal quantum numbers n . The transition frequency $\omega_{nn'}$ between the initial state n and the final state n' is given by the Rydberg formula:

$$\omega_{nn'} = R \left(\frac{1}{n^2} - \frac{1}{n'^2} \right) \quad (12)$$

Here, $R = e^4 m_e / 16\pi^2 \epsilon_0^2 \hbar^2$ is the Rydberg constant. We adopt atomic units [a.u.], defined by $1/4\pi\epsilon_0 = 1$, $e = 1$, and $m_e = 1$, under which the Rydberg constant becomes $R = 1/2$ [a.u.] = 13.6 [eV]. The optical transitions considered in this calculation are summarized in Table I. In the following β , γ_{α} , η_{α} , and ω are converted into atomic units for consistency. In other systems—such as color centers or ionic liquids—the Coulomb interaction is significantly weaker. As a result, the effective Rydberg constant in these models is one to two orders of magnitude lower than that of the hydrogen atom.

III. NUMERICAL DEMONSTRATIONS: LINEAR ABSORPTION SPECTRUM

We adopted 55 energy eigenstates, encompassing all eigenstates from principal quantum number $n = 1$ (1S) to $n = 5$ (5g). The number of hierarchical layers for each heat bath was set to $N_{\alpha} = 2$ using the Padé approximation of the [0/1] form.

We ran the AO-HEOM code using Python 3.13.5, along with CuPy 13.4.1 to enable CUDA support, NumPy 2.2.5, and SciPy 1.15.3 for special functions and numerical integration. To time-integrate the HEOM, we used the fourth-order Runge–Kutta method. For computing the transition matrix, we applied SciPy's quad function, which is based on the FORTRAN QUADPACK library.

The computations were performed on a system equipped with an Intel Core i9-13900KF CPU and an NVIDIA GeForce RTX 4090 GPU, using CUDA Toolkit version 11.8. Each simulation with 3000 time steps required approximately 2.4 GB of GPU memory and 20,000 seconds of computation time. The AO-HEOM source

code developed herein will be made publicly available in a separate work.

We consider the isotropic bath case, in which the inverse noise correlation times are uniformly set to $\gamma_x = \gamma_y = \gamma_z = 1$, and the coupling strengths are varied identically in all directions as $\eta_x = \eta_y = \eta_z = \eta$. The spectra were computed using Eq. (10) at inverse temperatures $\beta =$ (a) 1.0, (b) 2.0, and (c) 5.0. To highlight the role of thermal fluctuations and dissipation in a Coulomb potential system, we intentionally consider an unphysically high-temperature bath with relatively strong S–B coupling. For instance, in hydrogen, $\beta = 1.0$ corresponds to approximately 3×10^5 [K]. Note that the value of R is typically an order of magnitude lower for color centers. For ionic liquids, where the potential includes shielding effects, the temperature scale is reduced by up to two orders of magnitude. Therefore, for example, a low-temperature case such as $\beta = 5$ or lower can be realized experimentally.

A. Strong S-B coupling cases

Figure 1(a)-(c) presents the calculated results for relatively strong S–B coupling: (i) weak (solid curve, $\eta = 0.001$), (ii) intermediate (dashed curve, $\eta = 0.005$), and (iii) strong (dotted curve, $\eta = 0.01$).

The effect of the bath manifests in the fluctuation and dissipation related by the fluctuation-dissipation theorem, with only the fluctuation exhibiting temperature dependence.^{14,15} Thus, the effect of temperature alters not only the initial equilibrium distribution but also the correlation time and amplitude of fluctuations. This manifests as temperature dependence of the line profiles.

First, we discuss the high-temperature case in Fig. 1(a). At this temperature, thermal excitation populates high-energy states, leading to absorption peaks spanning a broad range of excitation transitions. (See the distribution of colored vertical lines derived from the golden rule.) The eigenstates of an atom are discrete, whereas the bath energy states are continuous. In the presence of S–B interaction, the atomic energy levels become effectively continuous due to “bathentanglement,” leading to broadened peaks from the mixing of atomic excited states. Temperature-dependent bath fluctuations further contribute to spectral broadening. In 2D spectroscopy, the effect of bathentanglement is observed as an echo peak.¹⁵

Alongside the broadening of the peaks, these results also exhibit a notable fading of the Paschen and Brackett series peaks (green and purple lines) in the low-frequency domain. This tendency becomes stronger as the S–B coupling increases, and in (iii) the strong coupling regime (dotted curve), only a single broadened peak, centered approximately in the Lyman region, is observed. As temperature and thermal coupling strength increase, the fluctuation amplitude grows. Consequently, transitions from large n to n' are strongly influenced due to the small

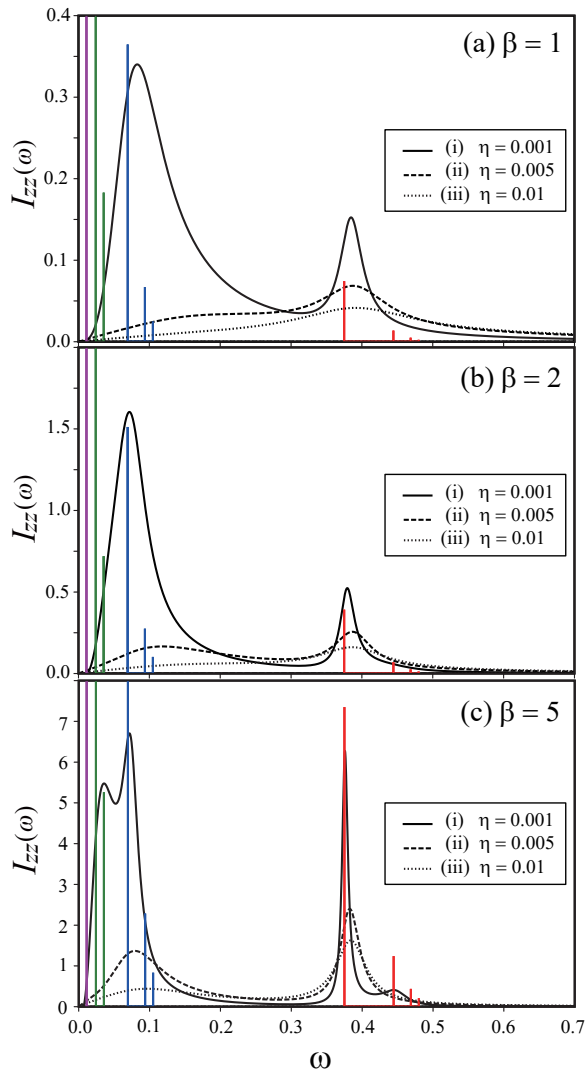


FIG. 1. Linear absorption spectra $I_{zz}(\omega)$ along the z direction for three temperature regimes: (a) high ($\beta = 1.0$), (b) intermediate ($\beta = 2.0$), and (c) low ($\beta = 5.0$). Each panel shows results for three S-B coupling strengths: (i) weak (solid curve, $\eta = 0.001$), (ii) intermediate (dashed curve, $\eta = 0.005$), and (iii) strong (dotted curve, $\eta = 0.01$). To provide a reference, the spectral intensity, evaluated via Fermi's Golden Rule [factors in Eq. (11)], was computed for each value of β and plotted after scaling by (a) 15, (b) 30, and (c) 100, to highlight the peak positions and relative intensities of each series. Among these, the red lines correspond to the Lyman series, the blue lines to the Balmer series, the green lines to the Paschen series, and the purple lines to the Brackett series.

transition frequency $\omega_{nn'}$.

To verify this point, we compared outcomes by increasing and decreasing the maximum principal quantum numbers n' in Appendix B. These results indicate that under strong S-B interaction at high temperatures, transitions from large n to n' exhibit semi-classical behavior,

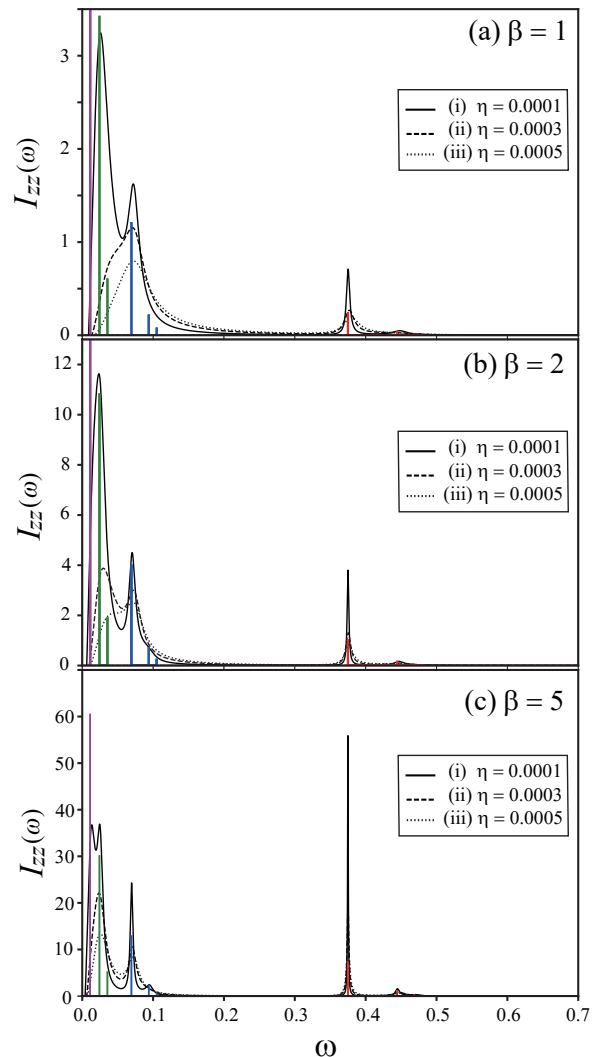


FIG. 2. Linear absorption spectra $I_{zz}(\omega)$ along the z direction. The calculation conditions are the same as in Fig. 1 (a)-(c), except that the SB bond strength is weakened as (i) $\eta = 0.0001$ (solid curve), (ii) $\eta = 0.0003$ (dashed curve), and (iii) $\eta = 0.0005$ (dotted curve). To provide a reference, the spectral intensity, evaluated via Fermi's Golden Rule [factors in Eq. (11)], was computed for each value of β and plotted after scaling by (a) 50, (b) 80, and (c) 100. Color-coded spectral lines: red for Lyman, blue for Balmer, green for Paschen, and purple for Brackett.

as they satisfy the condition $\beta\hbar\omega_{nn'} \ll 1$. Such a loss of quantum properties has been observed in quantum rotors and AB rings. Thus, regardless of whether the 3D-RISB or CL model is employed, only featureless semiclassical spectra are expected to emerge when either the QFPE or the high-temperature limit of the QHFPE is used, as exemplified by the AB ring case.^{36,37}

Figures 1(b) and (c) show the case where the temperature is lowered. In Fig. 1(c), when the SB interac-

tion is weak, the Paschen peak series appears following the Balmer series: The peak near $\omega = 0.08$ arises from the $2S \rightarrow 3P$ (Balmer- α) and $2S \rightarrow 4P$ (Balmer- β) transitions, whereas the peak near $\omega = 0.04$ arises from the $3S \rightarrow 4P$ (Paschen- α) transition. Accordingly, the peak near $\omega = 0.4$ corresponds to the $1S \rightarrow 2P$ (Lyman- α) transition. Additional transitions such as $1S \rightarrow 3P$ (Lyman- β) and $1S \rightarrow 4P$ (Lyman- γ) should appear at higher frequencies, but they are broadened and indistinct under the present physical conditions. The Balmer transition peak is prominent because the $2S$ state is well populated at this temperature. As in the case of Fig. 1(a), the Brackett series does not appear even at low temperature case in Fig. 1(c). This fact suggests that applying thermal baths can reduce the number of spectral transitions that need to be considered, thereby lowering computational costs.

B. Weak S-B coupling cases

Figure 2 presents results obtained by reducing the S-B coupling strength in the weakest case of Fig. 1 by a factor of 2 to 10. Because the S-B coupling is perturbative, the peaks of each series are more clearly observed. Note that our calculations do not employ the RWA and the FA, enabling an accurate treatment of thermal excitation. However, when applying the TCL-Redfield equation derived for the 3D-RISB model—non-Markovian yet using FA^{52,53}—positivity violations emerge beyond the case in Fig. 2 (a-i).⁴⁷ Thus, even in this weak coupling case, the perturbative approach, such as TCL-Redfield does not offer a meaningful alternative.

At high temperatures [Fig. 2(a)], reduced S-B coupling weakens fluctuation effects, sharpening the Lyman and Balmer peaks. The Paschen series also becomes visible due to enhanced low-frequency contributions. As the temperature lowers [Fig. 2(b) and (c)], fewer thermally excited states are populated, leading to diminished peak intensities for large n' . Yet, with fluctuations also suppressed, low-vibration transitions stand out more clearly—evident in the Brackett peak observed in Fig. 2(c-i).

Thus, lowering both the temperature and η sharpens the spectral peaks in Table I, affirming that the AO-HEOM framework aligns with physical intuition. While these results evoke the natural radiation damping theory^{10,11}; however, our approach extends beyond such treatments by non-perturbatively incorporating thermally structured environments. This enables the emergence of phenomena inaccessible to conventional models, such as the thermal suppression of high- n' transitions and the coherent merging of peaks across spectral series under strong coupling.

IV. CONCLUSION

We rigorously investigated the quantum mechanical effects of thermal fluctuations and dissipation in a Coulomb potential system using a Hamiltonian that incorporates the 3D-RISB model. Due to the uncertainty principle relating energy fluctuations to correlation times, quantum thermal noise must be treated as a non-Markovian process. Accordingly, we adopted the HEOM formalism, which provides a numerically “exact,” non-perturbative, non-Markovian description of system dynamics.

To validate this approach, we computed linear absorption spectra across a range of temperatures and S-B coupling strengths. When the S-B coupling is strong, Lyman and Balmer transitions dominate, and broadened peaks due to fluctuations are observed. As the temperature decreases or the S-B interaction weakens, Paschen and Brackett peaks, which are transitions from highly excited states, appear. This is because fluctuations due to temperature and S-B strength suppressed transitions with low excitation energy. It should be noted once again that when applying the CL model using a non-rotationally symmetric bath, the results exhibit classical behavior, and no quantum transition characteristics are observed.^{32,33}

Built on a kinetic equation governing energy exchange through thermal fluctuations and dissipation, our theory—grounded in the HEOM formalism—readily extends to the computation of higher-order nonlinear spectra, including 2D spectra^{14,15} and those arising under strong laser-field interactions.^{59,60} Moreover, it is also possible to include gauge fields,^{36,37} which would be useful for studying cavity QED.⁴²⁻⁴⁶

It should also be noted that AO-HEOM is applicable not only to systems with analytically determined eigenstates, such as $\propto -1/r + A/r^2$ with the centrifugal term A/r^2 added⁶¹⁻⁶³ or $\propto A/r^2 + \omega^2 r^2$ describing rotational-vibrational (with frequency ω) motion,^{64,65} but also to molecular systems using molecular orbitals obtained numerically. Future challenges include extending this approach to multi-electron systems defined in Fock space. We will continue such attempts in subsequent papers.

The AO-HEOM source code developed herein, which fully utilizes the graphics processing unit (GPU), will be made publicly available in a separate work.

ACKNOWLEDGMENTS

Y. T. was supported by JST (Grant No. CREST 1002405000170). Y. Z. is supported by JST SPRING, the establishment of university fellowships toward the creation of science technology innovation (Grant No. JPMJSP2110). Y. Z. thanks Shoki Koyanagi for providing useful information in the development of the HEOM program.

AUTHOR DECLARATIONS

Conflict of Interest

The authors have no conflicts to disclose.

DATA AVAILABILITY

The data that support the findings of this study are available from the corresponding author upon reasonable request.

Appendix A: Basis function of Coulomb potential system

The eigenfunction of Hamiltonian Eq.(2) in atomic units is expressed as a combination of associated Laguerre polynomials and spherical functions.

$$Y_l^m(\theta, \phi) = (-1)^{\frac{m+|m|}{2}} N_l^m e^{im\phi} P_l^{|m|}(\cos\theta) \quad (\text{A1})$$

with the normalization coefficient

$$N_l^m = \sqrt{\frac{2l+1}{4\pi} \frac{(l-m)!}{(l+m)!}} \quad (\text{A2})$$

and P_l^m are associated Legendre polynomials. Here, we adopt the following expressions:

$$Y_{lm}(\theta, \phi) = \sqrt{2} N_l^m \sin(|m|\phi) P_l^{|m|}(\cos\theta) \quad (m < 0) \quad (\text{A3})$$

and

$$Y_{lm}(\theta, \phi) = \sqrt{2} N_l^m \cos(|m|\phi) P_l^{|m|}(\cos\theta). \quad (m > 0) \quad (\text{A4})$$

The radial part is expressed as

$$R_{nl}(r) = \sqrt{\left(\frac{2A}{n}\right)^3 \frac{(n-l-1)!}{2n(n+l)!}} \times e^{-Ar/n} \left(\frac{2Ar}{n}\right)^l L_{n-l-1}^{(2l+1)}\left(\frac{2Ar}{n}\right), \quad (\text{A5})$$

where $L_{n-l-1}^{(2l+1)}$ are associated Laguerre polynomials.

Appendix B: Suppression of high excitation by baths

When the temperature of the thermal baths is high and the S-B coupling is strong, the contribution of spectral transitions from large n to n' is suppressed. This phenomenon is interpreted as a manifestation of strong thermal fluctuations suppressing low-frequency quantum transitions.

To illustrate this effect, we computed the absorption spectra for varying principal quantum numbers $n' = 2$ to 5, corresponding to a total eigenstate count ranging

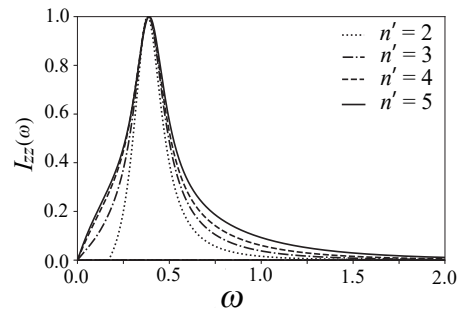


FIG. 3. Linear absorption spectra $I_{zz}(\omega)$ in the z direction for principal quantum numbers of the final state ranging from $n' = 2$ to 5. The inverse temperature and the S-B coupling are fixed at $\beta = 1.0$ and $\eta = 0.01$. Each curve is normalized to its maximum peak intensity.

from 5 to 55. The inverse temperature and S-B coupling strength were fixed at $\beta = 1.0$ and $\eta = 0.01$, respectively. All spectra were normalized to their maximum peak intensity for direct comparison.

As the basis set expands, the spectral profile stabilizes, with only minor shifts in peak positions. At elevated temperatures, many excited states above $n = 3$ become thermally accessible, and several transitions predicted by Fermi's golden rule are expected to appear. Yet, the overall spectral shape in this frequency range remains largely insensitive to n . This behavior results from the suppression of low-frequency transition processes induced by strong fluctuations. Discrete energy levels with small energy separations become effectively continuous and shift due to these fluctuations, leading to the attenuation of spectral peaks associated with them. The low-frequency regime, characterized by continuous resonance frequencies, satisfies the condition $\beta\hbar\omega_{nm'} \ll 1$, allowing a semiclassical interpretation reminiscent of pre-Bohr dynamics—where frictional forces reduce angular momentum and draw the particle toward the potential center. In this regime, no distinct peaks appear in the low-frequency region.

¹I. Tugov, On the Theory of Coulomb Interaction, NASA technical translation (National Aeronautics and Space Administration, 1967).

²H. Van Haeringen, "Charged-particle interactions: theory and formulas," (1985).

³M. Klein, Classical Planar Scattering by Coulombic Potentials, Lecture Notes in Physics Monographs, Vol. 13 (Springer, 2014) p. 147.

⁴D. G. Kanhere, A. Farazdel, and V. H. Smith, "Positron annihilation from F centers of alkali halide crystals," *Phys. Rev. B* **35**, 3131–3137 (1987).

⁵C. K. Ong, "Lattice static calculation of F-centre absorption energy in caesium halides," *Journal of Physics C: Solid State Physics* **15**, 427 (1982).

⁶T. Muto, "Theory of the F-centers of coloured alkali halide crystals. part i structure of f-absorption bands*," *Progress of Theoretical Physics* **4**, 181–192 (1949).

⁷K. Seddon, Quill Handbook of Ionic Liquid (Quill, 2008) first published in 2008.

- ⁸W. Freyland, *Coulombic Fluids: Bulk and Interfaces*, Springer Series in Solid-State Sciences (Springer Berlin Heidelberg, 2011).
- ⁹A. A. Othman, M. de Montigny, and F. Margiglio, “The Coulomb potential in quantum mechanics revisited,” *American Journal of Physics* **85**, 346–351 (2017), https://pubs.aip.org/aapt/ajp/article-pdf/85/5/346/13077589/346_1_online.pdf.
- ¹⁰M. O. Scully and W. E. Lamb, “Quantum theory of an optical maser. I. general theory,” *Phys. Rev.* **159**, 208–226 (1967).
- ¹¹B. Mollow and M. Miller, “The damped driven two-level atom,” *Annals of Physics* **52**, 464–478 (1969).
- ¹²Y. Tanimura and R. Kubo, “Time evolution of a quantum system in contact with a nearly Gaussian-Markoffian noise bath,” *Journal of the Physical Society of Japan* **58**, 101–114 (1989).
- ¹³A. Ishizaki and Y. Tanimura, “Quantum dynamics of system strongly coupled to low-temperature colored noise bath: Reduced hierarchy equations approach,” *Journal of the Physical Society of Japan* **74**, 3131–3134 (2005).
- ¹⁴Y. Tanimura, “Stochastic Liouville, Langevin, Fokker-Planck, and master equation approaches to quantum dissipative systems,” *Journal of the Physical Society of Japan* **75**, 082001 (2006).
- ¹⁵Y. Tanimura, “Numerically ”exact” approach to open quantum dynamics: The hierarchical equations of motion (HEOM),” *The Journal of Chemical Physics* **153**, 020901 (2020).
- ¹⁶A. J. Leggett, S. Chakravarty, A. T. Dorsey, M. P. A. Fisher, A. Garg, and W. Zwerger, “Dynamics of the dissipative two-state system,” *Rev. Mod. Phys.* **59**, 1–85 (1987).
- ¹⁷R. Silbey and R. A. Harris, “Variational calculation of the dynamics of a two level system interacting with a bath,” *The Journal of Chemical Physics* **80**, 2615–2617 (1984).
- ¹⁸C. Hsieh, J. Liu, C. Duan, and J. Cao, “A nonequilibrium variational polaron theory to study quantum heat transport,” *The Journal of Physical Chemistry C* **123**, 17196–17204 (2019).
- ¹⁹S. Koyanagi and Y. Tanimura, “Thermodynamic quantum Fokker-Planck equations and their application to thermostatic Stirling engine,” *The Journal of Chemical Physics* **161**, 112501 (2024), [arXiv:2408.01083](https://arxiv.org/abs/2408.01083).
- ²⁰S. Koyanagi and Y. Tanimura, “Hierarchical equations of motion for multiple baths (HEOM-MB) and their application to Carnot cycle,” *The Journal of Chemical Physics* **161**, 162501 (2024), [arXiv:2408.02249](https://arxiv.org/abs/2408.02249).
- ²¹H.-P. Breuer and F. Petruccione, *The theory of open quantum systems* (Oxford:Oxford University Press, 2002) pp. xxi + 625.
- ²²U. Weiss, *Quantum Dissipative Systems*, 4th ed. (WORLD SCIENTIFIC, 2012).
- ²³E. Geva and R. Kosloff, “A quantum-mechanical heat engine operating in finite time. a model consisting of spin-1/2 systems as the working fluid,” *The Journal of chemical physics* **96**, 3054–3067 (1992).
- ²⁴S. Deffner and S. Campbell, “Quantum thermodynamics: An introduction to the thermodynamics of quantum information,” (2019).
- ²⁵A. G. Redfield, “The theory of relaxation processes,” in *Advances in Magnetic and Optical Resonance*, *Advances in Magnetic and Optical Resonance*, Vol. 1 (Academic Press, 1965) pp. 1–32.
- ²⁶A. Caldeira and A. Leggett, “Path integral approach to quantum brownian motion,” *Physica A: Statistical Mechanics and its Applications* **121**, 587–616 (1983).
- ²⁷L. D. Chang and D. Waxman, “Quantum Fokker-Planck equation,” *Journal of Physics C: Solid State Physics* **18**, 5873 (1985).
- ²⁸N. Makri, “Numerical path integral techniques for long time dynamics of quantum dissipative systems,” *Journal of Mathematical Physics* **36**, 2430–2457 (1995), https://pubs.aip.org/aip/jmp/article-pdf/36/5/2430/19149255/2430_1_online.pdf.
- ²⁹N. Makri and D. E. Makarov, “Tensor propagator for iterative quantum time evolution of reduced density matrices. i. theory,” *The Journal of Chemical Physics* **102**, 4600–4610 (1995), https://pubs.aip.org/aip/jcp/article-pdf/102/11/4600/19014630/4600_1_online.pdf.
- ³⁰N. Makri and D. E. Makarov, “Tensor propagator for iterative quantum time evolution of reduced density matrices. ii. numerical methodology,” *The Journal of Chemical Physics* **102**, 4611–4618 (1995), https://pubs.aip.org/aip/jcp/article-pdf/102/11/4611/19015655/4611_1_online.pdf.
- ³¹Y. Suzuki and Y. Tanimura, “Quantum theory of a two-dimensional rotator in a dissipative environment: Application to far-infrared spectroscopy,” *Journal of the Physical Society of Japan* **70**, 1167–1170 (2001).
- ³²Y. Suzuki and Y. Tanimura, “Two-time correlation function of a two-dimensional quantal rotator in a colored noise,” *Journal of the Physical Society of Japan* **71**, 2414–2426 (2002).
- ³³Y. Iwamoto and Y. Tanimura, “Linear absorption spectrum of a quantum two-dimensional rotator calculated using a rotationally invariant system-bath Hamiltonian,” *The Journal of Chemical Physics* **149**, 084110 (2018).
- ³⁴Y. Iwamoto and Y. Tanimura, “Open quantum dynamics of a three-dimensional rotor calculated using a rotationally invariant system-bath Hamiltonian: Linear and two-dimensional rotational spectra,” *The Journal of Chemical Physics* **151**, 044105 (2019).
- ³⁵L. Chen, M. F. Gelin, and W. Domcke, “Orientational relaxation of a quantum linear rotor in a dissipative environment: Simulations with the hierarchical equations-of-motion method,” *The Journal of Chemical Physics* **151**, 034101 (2019).
- ³⁶H. Yang, S. Koyanagi, and Y. Tanimura, “Quantum hierarchical Fokker-Planck equations with U(1) gauge fields: Application to the Aharonov-Bohm ring,” *The Journal of Chemical Physics* **163**, 144107 (2025), <https://arxiv.org/abs/2509.11462>.
- ³⁷S. Koyanagi, H. Yang, and Y. Tanimura, “Quantum hierarchical Fokker-Planck equations with U(1) gauge fields (U(1)-QHPE): A computational framework for Aharonov-Bohm effects,” *The Journal of Chemical Physics* (2025), <https://arxiv.org/abs/2509.11195>.
- ³⁸Y. Gefen, E. Ben-Jacob, and A. O. Caldeira, “Zener transitions in dissipative driven systems,” *Phys. Rev. B* **36**, 2770–2782 (1987).
- ³⁹J. M. Raimond, M. Brune, and S. Haroche, “Manipulating quantum entanglement with atoms and photons in a cavity,” *Rev. Mod. Phys.* **73**, 565–582 (2001).
- ⁴⁰I. M. Georgescu, S. Ashhab, and F. Nori, “Quantum simulation,” *Rev. Mod. Phys.* **86**, 153–185 (2014).
- ⁴¹P. Forn-Díaz, L. Lamata, E. Rico, J. Kono, and E. Solano, “Ultrastrong coupling regimes of light-matter interaction,” *Rev. Mod. Phys.* **91**, 025005 (2019).
- ⁴²O. D. Stefano, A. Settineri, V. Macrì, L. Garziano, R. Stassi, S. Savasta, and F. Nori, “Resolution of gauge ambiguities in ultrastrong-coupling cavity quantum electrodynamics,” *Nature Physics* **15**, 803–808 (2019).
- ⁴³L. Garziano, A. Settineri, O. Di Stefano, S. Savasta, and F. Nori, “Gauge invariance of the dicke and hopfield models,” *Phys. Rev. A* **102**, 023718 (2020).
- ⁴⁴S. Savasta, O. Di Stefano, A. Settineri, D. Zueco, S. Hughes, and F. Nori, “Gauge principle and gauge invariance in two-level systems,” *Phys. Rev. A* **103**, 053703 (2021).
- ⁴⁵K. Akbari, W. Salmon, F. Nori, and S. Hughes, “Generalized dicke model and gauge-invariant master equations for two atoms in ultrastrongly-coupled cavity quantum electrodynamics,” *Phys. Rev. Res.* **5**, 033002 (2023).
- ⁴⁶Q. Bin, Y. Wu, J.-H. Gao, A. Chen, F. Nori, and X.-Y. Lü, “Cavity QED based on strongly localized modes: exponentially enhancing single-atom cooperativity,” *Physical Review Letters* **135** (2025), 10.1103/PhysRevLett.135.103602, [arXiv:2509.04739](https://arxiv.org/abs/2509.04739) [quant-ph].
- ⁴⁷Y. Tanimura, “Real-time and imaginary-time quantum hierarchical Fokker-Planck equations,” *The Journal of Chemical Physics* **142**, 144110 (2015).

- ⁴⁸T. Ikeda, A. G. Dijkstra, and Y. Tanimura, "Modeling and analyzing a photo-driven molecular motor system: Ratchet dynamics and non-linear optical spectra," *The Journal of Chemical Physics* **150**, 114103 (2019).
- ⁴⁹C. Kreisbeck, T. Kramer, M. Rodríguez, and B. Hein, "High-performance solution of hierarchical equations of motion for studying energy transfer in light-harvesting complexes," *Journal of Chemical Theory and Computation* **7**, 2166–2174 (2011), PMID: 26606486, <https://doi.org/10.1021/ct200126d>.
- ⁵⁰M. Tsuchimoto and Y. Tanimura, "Spins dynamics in a dissipative environment: Hierarchical equations of motion approach using a Graphics Processing Unit (GPU)," *Journal of Chemical Theory and Computation* **11**, 3859–3865 (2015).
- ⁵¹A. Ishizaki and Y. Tanimura, "Nonperturbative non-Markovian quantum master equation: Validity and limitation to calculate nonlinear response functions," *Chemical Physics* **347**, 185–193 (2008), *ultrafast Photoinduced Processes in Polyatomic Molecules*.
- ⁵²F. Shibata, Y. Takahashi, and N. Hashitsume, "A generalized stochastic liouville equation. non-markovian versus memoryless master equations," *Journal of Statistical Physics* **17**, 171–187 (1977).
- ⁵³S. Chaturvedi and F. Shibata, "Time-convolutionless projection operator formalism for elimination of fast variables. applications to brownian motion," *Zeitschrift für Physik B Condensed Matter* **35**, 297–308 (1979).
- ⁵⁴L. D. Zusman, "Outer-sphere electron transfer in polar solvents," *Chemical Physics* **49**, 295–304 (1980).
- ⁵⁵Q. Shi, L. Chen, G. Nan, R. Xu, and Y. Yan, "Electron transfer dynamics: Zusman equation versus exact theory," *The Journal of Chemical Physics* **130**, 164518 (2009).
- ⁵⁶Y. Tanimura and P. G. Wolynes, "Quantum and classical Fokker-Planck equations for a Gaussian-Markovian noise bath," *Phys. Rev. A* **43**, 4131–4142 (1991).
- ⁵⁷H. Takahashi and Y. Tanimura, "Open quantum dynamics theory of spin relaxation: Application to μ sr and low-field NMR spectroscopies," *Journal of the Physical Society of Japan* **89**, 064710 (2020).
- ⁵⁸J. Hu, R.-X. Xu, and Y. Yan, "Communication: Padé spectrum decomposition of Fermi function and Bose function," *The Journal of Chemical Physics* **133**, 101106 (2010).
- ⁵⁹Y. Tanimura and S. Mukamel, "Optical Stark spectroscopy of a Brownian oscillator in intense fields," *Journal of the Physical Society of Japan* **63**, 66–77 (1994).
- ⁶⁰M. F. Gelin, Y. Tanimura, and W. Domcke, "Simulation of femtosecond "double-slit" experiments for a chromophore in a dissipative environment," *The Journal of Chemical Physics* **139**, 214302 (2013).
- ⁶¹H. Bethe, "Zur theorie der metalle. I. eigenwerte und eigenfunktionen der linearen atomkette," *Zeitschrift für Physik* **71**, 205–226 (1931).
- ⁶²L. Pauling, "The theoretical prediction of the physical properties of many-electron atoms and ions. I. the ground state," *Proceedings of the National Academy of Sciences* **12**, 473–479 (1926).
- ⁶³L. D. Landau and E. M. Lifshitz, "Quantum mechanics: Non-relativistic theory," *Course of Theoretical Physics*, **3** (1977).
- ⁶⁴F. Calogero, "Ground state of a one-dimensional n body system," *Journal of Mathematical Physics* **10**, 2191–2196 (1969).
- ⁶⁵F. Calogero, "Solution of a three-body problem in one dimension," *Journal of Mathematical Physics* **12**, 419–424 (1971).